Intermetallics, Volume 122, July 2020, Article 106795
DOI: 10.1016/j.intermet.2020.106795

An atomistic study of the structural changes in a Zr-Cu-Ni-Al glass-forming liquid on vitrification monitored in-situ by X-ray diffraction and molecular dynamics simulation

D. V. Louzguine-Luzgin[1,2&], K. Georgarakis[3], J. Andrieux[4,5], L. Hennet[6], T. Morishita[2], K. Nishio[2] and R.V. Belosludov[7]

[1] *WPI Advanced Institute for Materials Research, Tohoku University, Aoba-Ku, Sendai 980-8577, Japan*

[2] *MathAM-OIL, National Institute of Advanced Industrial Science and Technology (AIST), Sendai 980-8577, Japan*

[3] *School of Aerospace, Transport and Manufacturing, Cranfield University, Cranfield, MK43 0AL, UK*

[4] *European Synchrotron Radiation Facility, 38042, Grenoble, France*

[5] *Laboratoire des Multimatériaux et Interfaces, UMR CNRS 5615, Univ Lyon, Université Claude Bernard Lyon 1, F-69622 Villeurbanne, France*

[6] *CNRS-CEMHTI, University of Orleans, 45071 Orleans Cedex 02, France*

[7] *Institute for Materials Research, Tohoku University, Aoba-Ku, Sendai 980-8577, Japan*

Abstract

Structural changes in the $Zr_{55}Cu_{30}Ni_5Al_{10}$ liquid alloy on cooling from above the equilibrium liquidus temperature are studied by synchrotron radiation X-ray diffraction and compared with the results of first-principles molecular dynamics simulation. In-situ vitrification of the studied alloy is achieved using a containerless levitation technique. Subsequent analysis of the atomic and electronic structure of the alloy in liquid and glassy states reveals formation of medium-range order on cooling and its relationship with liquid fragility. The structural changes in this alloy are smaller in comparison with a more fragile one.

Keywords: metallic glass; liquid; fragility; X-ray diffraction; structure; synchrotron radiation

[&] Corresponding author, Tel: +081-22-217-5957, Fax: +081-22-217-5957, E-mail: dml@wpi-aimr.tohoku.ac.jp

1. Introduction

The high glass-forming ability (GFA) of some alloy compositions allowed production of bulk metallic glasses (BMGs) (also called glassy alloys) in the thickness range of 1-100 mm using various casting processes [1,2]. Zr-based BMGs are among the best metallic glass-formers known to date [1-3] which thermal stability is also good [4]. Formation of a glassy phase in both Zr–Cu and Zr–Ni alloys is strongly enhanced by the addition of Al thus forming ternary and quaternary bulk metallic glasses with good glass-forming ability [1-5]. The atomic structure of these BMGs at room temperature was studied in detail [6,7].

Liquids retain their volume as crystals but flow under the action of gravity [8,9]. They constantly undergo a restructuring of the atomic structure [10,11]. Above the equilibrium liquidus temperature (T_l) and slightly below it metallic melts show nearly Arrhenius-type temperature dependence of viscosity (η):

$$\eta = \eta_0 \exp(E_a / RT) \qquad (1)$$

where η_0 is a pre-exponential factor, R is the gas constant and E_a is an activation energy [12]. However, on cooling below the liquidus temperature, starting from a crossover temperature [13], they exhibit a non-Arrhenius temperature dependence on viscosity which is known as *fragility* of liquids [14,15].

Here one should mention that anomalous variation in a liquid viscosity in the vicinity of T_l and above it was observed for Fe- [16,17] and Zr- based glass-forming alloys [18] as well as for Al-based crystalline alloys [19]. The authors stated that liquid metallic alloys can have various structural states and significant overheating is required to dissolve clusters inherited from the solid state and to reach equilibrium liquid structure. The existence of liquid-liquid transitions in deeply supercooled state found for water [20], molecular liquids [21,22] (confirmed by computer simulation [23]) and even metallic glasses [24] should also be taken into account when describing fragility.

The inverse temperature - logarithmic viscosity plot [25,26] with some limitations [27,28] is a very useful illustration of the difference between so-called "strong" and "fragile" liquids [29,30]. Fragility is also related to the glass-forming ability of BMGs [31,32] (with some argumentation [33])

partly because stronger liquids, in general, have a higher viscosity in the entire temperature range from T_l and T_g. There are also experimental results which indicate correlation between liquid fragility and vibrational properties of the glass below T_g [34]. The fragility index (m) [35,36] of the supercooled liquid is calculated slightly above the glass-transition temperature (T_g) as a derivative:

$$m=d\log(\eta)/d(T_g/T) \quad (2).$$

Another way of representation of fragility is a famous Vogel-Fulcher-Tammann-Hesse equation [1]:

$$\eta=\eta_0 exp[D^*T_0/(T-T_0)] \quad (3)$$

where η_0, D (as an indicator of the fragility) and T_0 are the fitting parameters. This equation is widely used but describes the temperature dependence of viscosity well only in an intermediate temperature region [37]. While some other equations make a better representation of the entire viscosity plot [38,39] they have a larger number of fitting parameters which physical meaning could be less clear.

On the other hand fragility can be expressed by the ratio of the activation energies for viscous flow in the equation (1) at low (E_L), (close to T_g) and high (E_H) temperature region (slightly above T_l) [40,41]:

$$R_D= E_L/E_H \quad (4).$$

Other methods are also used to describe and separate thermodynamic and kinetic fragility [42].

Metallic glasses exhibit structural changes in the supercooled liquid state and such changes are found to be responsible for the liquid fragility. A relatively fragile $Pd_{42.5}Cu_{30}Ni_{7.5}P_{20}$ melt (its fragility index m is close to 60 [43]) during cooling was studied by using the real-space pair distribution function (G) (which is a reduced radial distribution function (RDF)) [44] and compared to the results obtained by the first-principles calculations. As a result strong correlation between the structural changes and the variation of viscosity was observed in the supercooled liquid [45]. The rate of structural rearrangements on cooling was enhanced in the supercooled liquid close to T_g. It was also demonstrated for Ni–Nb–Ta [46] and other [47,48] liquid alloys.

Structural changes, thermal expansion and volume changes (structural relaxation) in Zr-based metallic glasses upon heating [49,50] and cooling [51] were studied by synchrotron X-ray radiation

diffraction and transmission electron microscopy [52,53]. Recently it was shown that even scanning tunneling microscopy allows achieving atomic scale resolution for metallic glasses [54].

Zr-Cu(Ni)-Al alloys are among the most studied bulk metallic glasses [55]. A detailed study on vitrification of a ternary $Zr_{60}Cu_{30}Al_{10}$ alloy was performed recently in-situ by high energy synchrotron radiation X-ray diffraction from above the liquidus T_l to room temperature [56]. Short (SRO) and medium range order (MRO) develop significantly during cooling the liquid phase to the glassy state. Significant glassy structure and volume changes are found during severe plastic deformation [57] and rolling [58]. Structural changes in Cu-Zr [59,60] and Cu-Zr-Al glasses [61] were also studied by MD computer simulation.

Here we study the atomic structure changes in a relatively *strong* $Zr_{55}Cu_{30}Ni_5Al_{10}$ glass-forming liquid (one of the best glass-formers [62]) on vitrification and compare the results with those obtained for *fragile* metallic glasses. Its measured fragility parameter *m* for this liquid varies from about 45 [63,64] to 29 [65] but it is lower than that obtained for the Pd-Cu-Ni-P one studied earlier.

2. Experimental Procedure

An ingot of the $Zr_{55}Cu_{30}Ni_5Al_{10}$ alloy (the composition is given in nominal atomic percentage) was prepared from pure metals of more than 99.9 mass% purity using the arc-melting method. Thermal stability of the samples was tested using a differential scanning calorimeter (DSC).

In-situ X-ray diffraction experiments were carried out at the European Synchrotron Radiation Facility (ESRF). The incident beam wavelength was 0.1245 Å (100 keV). Diffraction spectra were acquired in transmission mode by a 2D detector. An aerodynamic levitation setup [66] was used to heat up, melt and cool down the metallic glass spheres in situ under synchrotron radiation. The spheres were levitating by high purity argon flowing through an aluminum nozzle and melted using two CO_2 laser beams. Two pyrometers were used to record the temperature while temperature values below 620 K were calculated. Diffraction intensities were recorded during cooling with a time resolution of 100 ms. The radial intensities were integrated over 90 degrees (1/4 of the entire halo) to

obtain one-dimensional spectrum and enhance the signal to noise ratio. The accuracy of the temperature values is estimated at ±10 K for the data above 900 K and better than ±7 K below 900 K.

After necessary corrections the measured intensity was converted to electron units per atom with the generalized Krogh-Moe-Norman method [67]. The density value of 6800 kg/m^3 for the alloy was obtained from Ref. [68]. The total structure factor *S(Q)* and the interference function *Qi(Q)* ($Q = 4\pi\sin\theta/\lambda$, θ is the diffraction angle) were obtained from the coherent scattering intensity by using atomic scattering factors. The radial distribution *RDF(R)* and pair distribution functions *G(R)* were obtained by the Fourier transform of *Qi(Q)* [67]. The maximum scattering vector (Q) value obtained was 250 nm^{-1}. However, as the noise level at high Q values was rather high the Fourier Transform was performed only until 150 nm^{-1}. Termination of the Fourier Transform at higher Q_{max} values was found to increase the noise of G(r) without any positive effect on the curves.

The atomic structure of the $Zr_{55}Cu_{30}Ni_5Al_{10}$ alloy in both liquid and glassy states was also modeled using the first-principles molecular dynamics simulation. The calculations were performed using density functional theory based pseudopotential plane-wave method as implemented in VASP code [69]. The atomic configuration was modeled within a cubic supercell consisting of 500 atoms. The spin polarized generalized gradient corrected Perdew-Burke-Ernzerhof exchange-correlation functional [70] and the projector augmented wave method [71] were used in order to accurately describe the interaction between the ion and electron. The Brillouin zone integrations were carried out using the Γ-point. At the first step, the random atomic structure was melted at 2000 K for a total of 10 ps. After that, the obtained system in liquid state was additionally equilibrated for 10 ps at 1400 K and 1000 K. The additional volume relaxations were performed for these structures using stress tensor calculation. In order to obtain the structures at lower temperatures owing to slower relaxation the cell obtained at 1000 K was cooled down to 800 K and then to 500 K with a cooling rate of 2×10^{14} K/s. The volume optimization was done for structures at 800 K and 500 K. After cell optimizations, all structures were equilibrated again for 2.5 ps at the same temperatures, respectively. The calculation of electron density of states were performed using enlarged Brillouin zone of 6 × 6 × 6 in order to get denser electron coverage.

3. Results and discussion

The alloy sample was heated up, melted and then cooled down at about 85 K/s (average cooling rate) from 1335 K (T_l ~ 1150 K [72]) to 388 K and the alloy vitrified. The measured intensity and the structure factor profiles obtained at two temperatures are shown in Fig. 1a. The glass-transition temperature measured by DSC at the heating rate of 0.67 K/s was about 680 K. This value is close to those found in the earlier works [68,73].

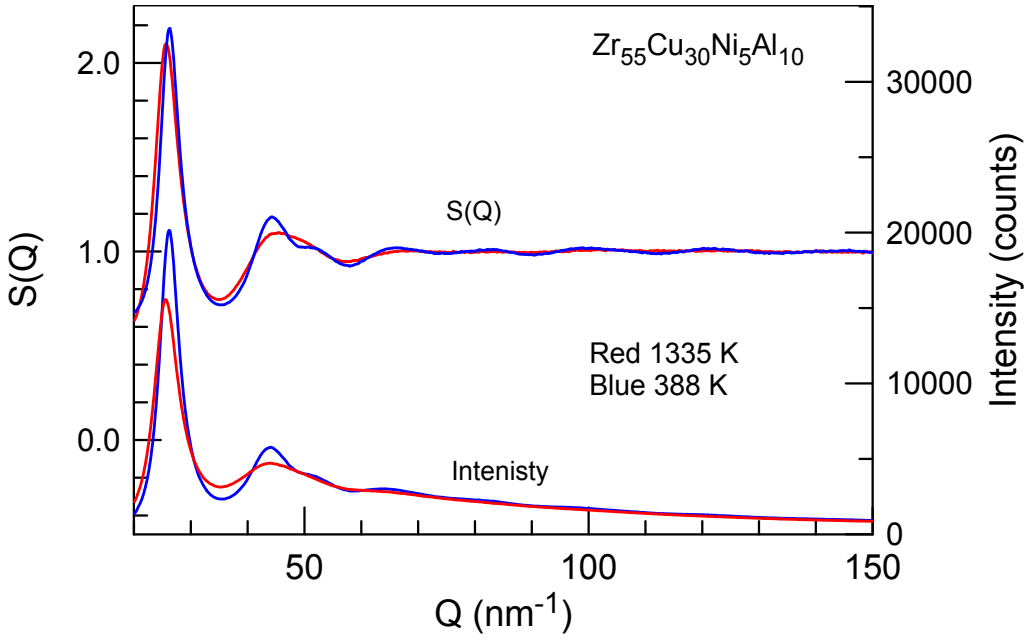

(a)

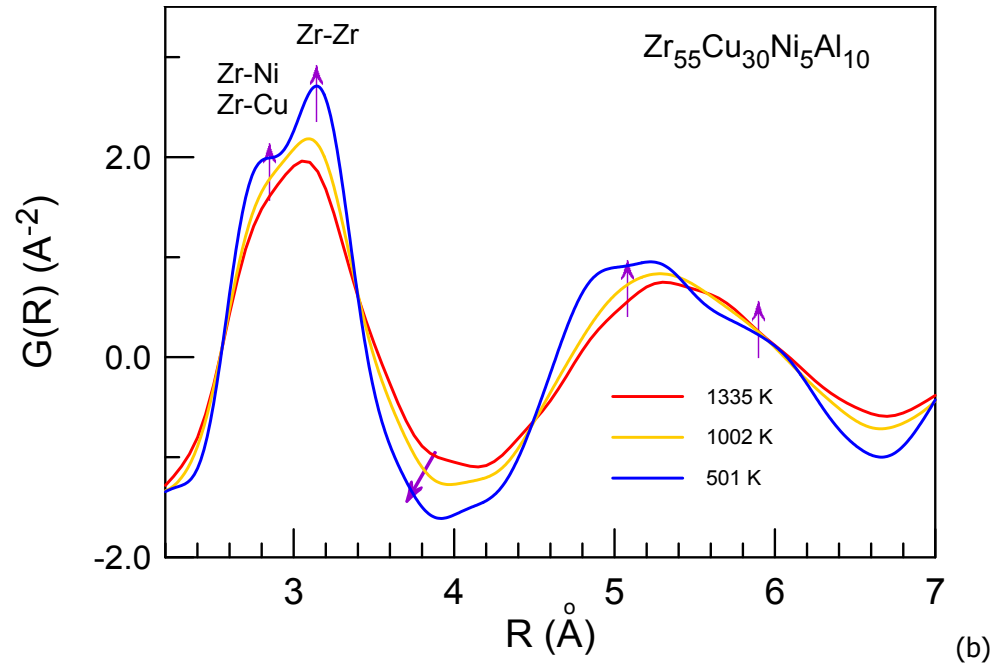

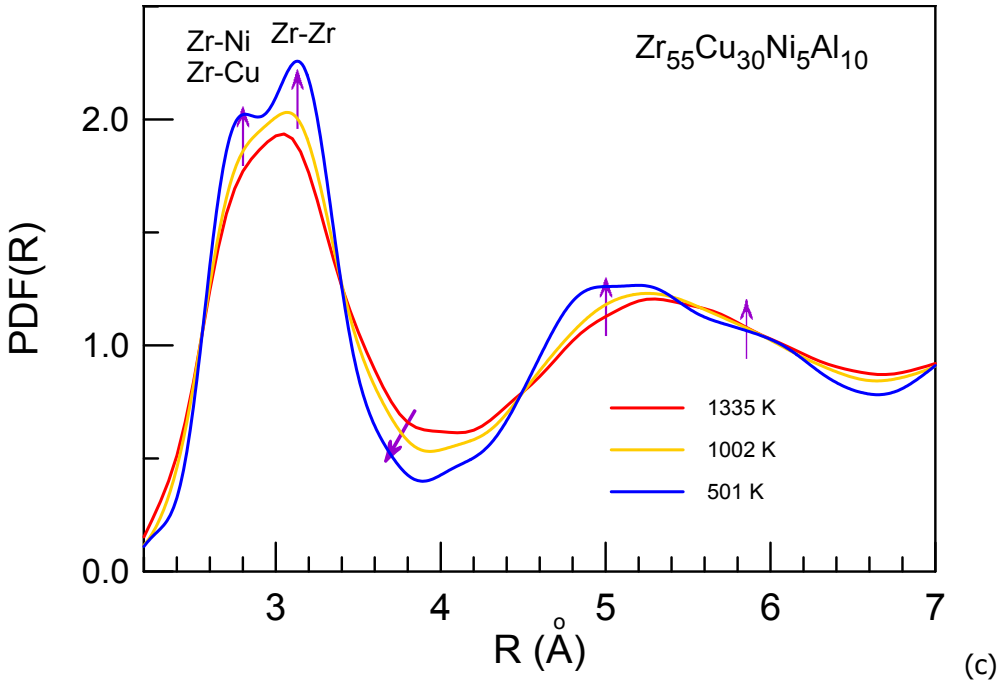

Fig. 1. (a) The experimental structure factor *S(Q)* at 1335 and 388 K calculated from the corresponding XRD intensity profile after the necessary corrections. (b) three typical *G(R)* functions and (c) three typical *PDF(R)* functions. Violet arrows (upward) show intensification of two sub-peaks responsible for Zr-(Cu,Ni) and Zr-Zr atomic interactions in the first

coordination shell and two sub-peaks at 0.5 and 0.58 nm in the second coordination shell. The arrow focusing downward-left indicates a decrease in the number of high R value interatomic distance on cooling.

Three typical *G(R)* graphs are shown in Fig. 1b. Pair distribution function profiles (*PDF(R)*) calculated using the following equation:

$$PDF(R) = G(R)/(4\pi\rho_0 R) + 1, \quad (5)$$

where ρ_0 is the atomic number density, are also shown in Fig. 1c. In order to separate influence of different atomic pairs the *G(R)* peaks were fitted with the several Gaussian functions. Fitting of four *G(R)* maxima (the baseline was corrected to make both outermost points of each coordination shell maximum be equal to zero) using 7 Gaussian peak functions produced a reasonable correspondence with the original *G(R)* plot (Fig. 2a). The temperature dependence of the center of mass position of 7th peak (4th coordination shell) indicates linear thermal contraction on cooling with a linear thermal expansion coefficient (a_l) of $2.8 \cdot 10^{-5}$ K^{-1} in the liquid and of $1.3 \cdot 10^{-5}$ K^{-1} in the glassy state (Fig. 2b). These values are quite close to those obtained by density measurements [68].

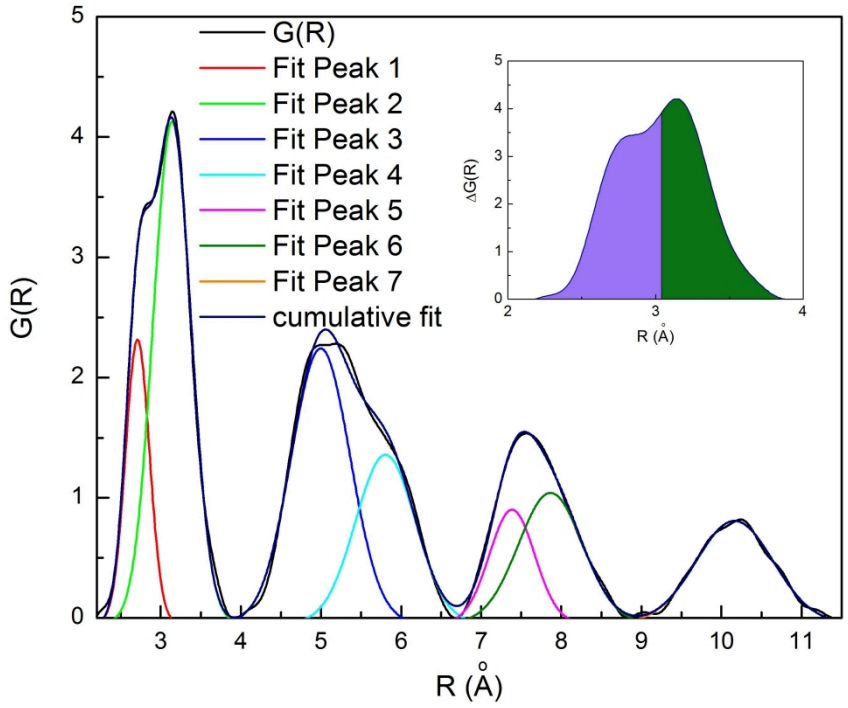
G(R)
Fit Peak 1
Fit Peak 2
Fit Peak 3
Fit Peak 4
Fit Peak 5
Fit Peak 6
Fit Peak 7
cumulative fit
G(R)
R (Å)
ΔG(R)
R (Å)

(a)

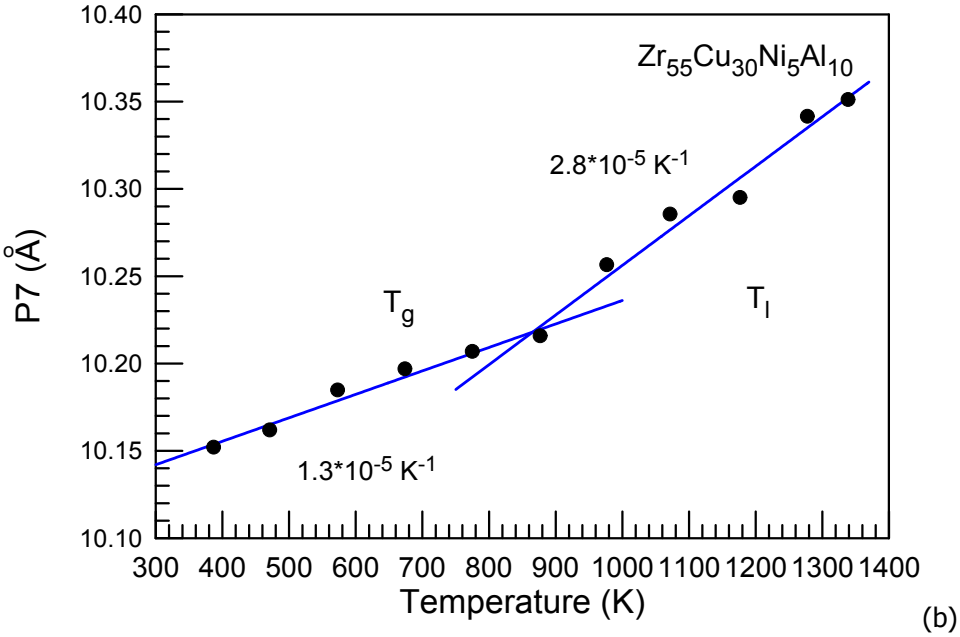
Zr55Cu30Ni5Al10
2.8*10-5 K-1
1.3*10-5 K-1
Tg
Tl
P7 (Å)
Temperature (K)

(b)

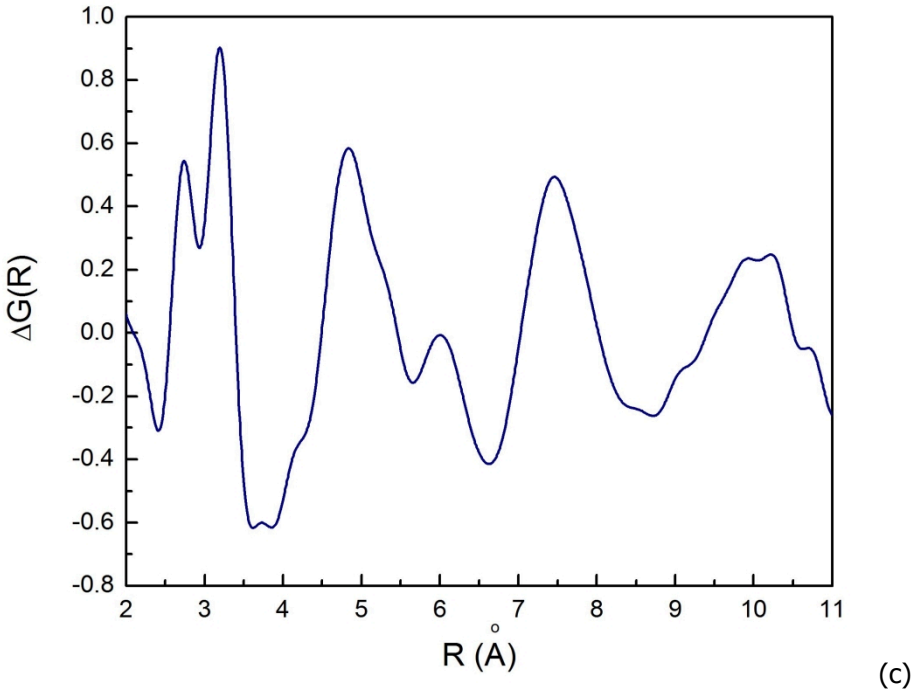

(c)

Fig. 2. Fitting of four *G(R)* maxima (black curve) from 0.23 to 1.15 nm obtained at 501 K using seven Gaussian functions related to P1 – P7 (as indicated) (a). The baseline was subtracted prior to fitting according to the minima at about 2.2, 4, 6.7, 9 and 11.5 A. The inset shows R^{i}_{50} value at which two areas A1 and A2 (purple and green) are equal. The positions of P7 as a function of temperature (b). The intensity difference between the *G(R)* curves at 501 and 1335 K before the baseline correction (c).

As one can see the first and second *G(R)* maxima clearly split in two sub-peaks (P1 and P2), especially at a low temperature. It is quite common for metallic glasses. A sub-peak at low *R* (P1) of about 0.271 nm is clearly visible on the first *G(R)* nearest neighbor (NN) peak. The intensity difference between two G(R) functions (Fig. 2c) indicates intensification of the sub-peaks at 0.272, 0.318 and 0.482 nm, etc… on cooling.

Opposite to the peaks related to other coordination shells (3rd, 4th, etc...) P1 and P2 of the first coordination shell shift to higher values on undercooling (Fig. 3a) as was found earlier for the Pd-Cu-Ni-P [74,75], Pd-Si [76], Cu-Zr [77], Zr-Cu-Ni-Al [78], Fe-B [79], many other alloys [80] as well as for

pure metals [81]. On cooling the present Zr-Cu-Ni-Al liquid alloy exhibits contraction in 3rd (P5 and P6) and 4th (P7) coordination shells (Fig. 2b). The peak position in the 2nd coordination shell, in general, did not change with temperature. Although P3 and P4 move in opposite directions (Fig. 3c) the average center of mass value of P3 and P4 is about 0.54 nm in the entire temperature range.

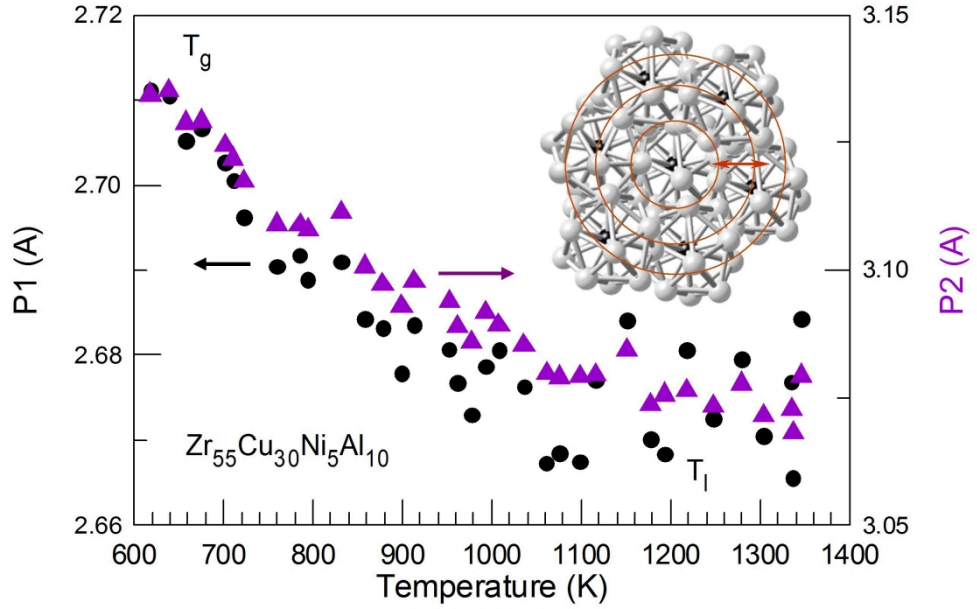

(a)

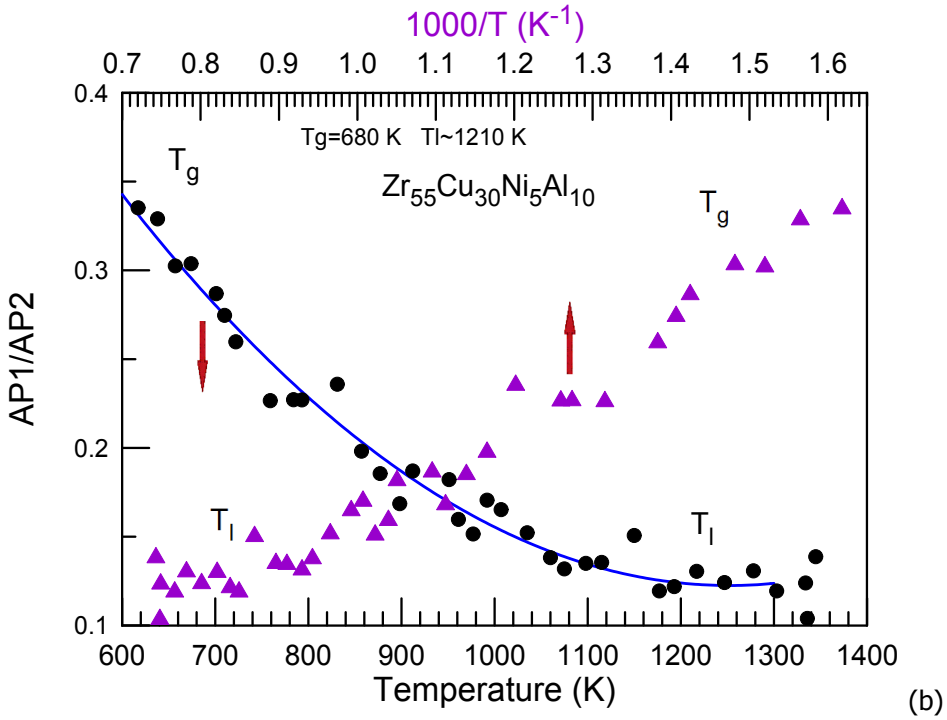

(b)

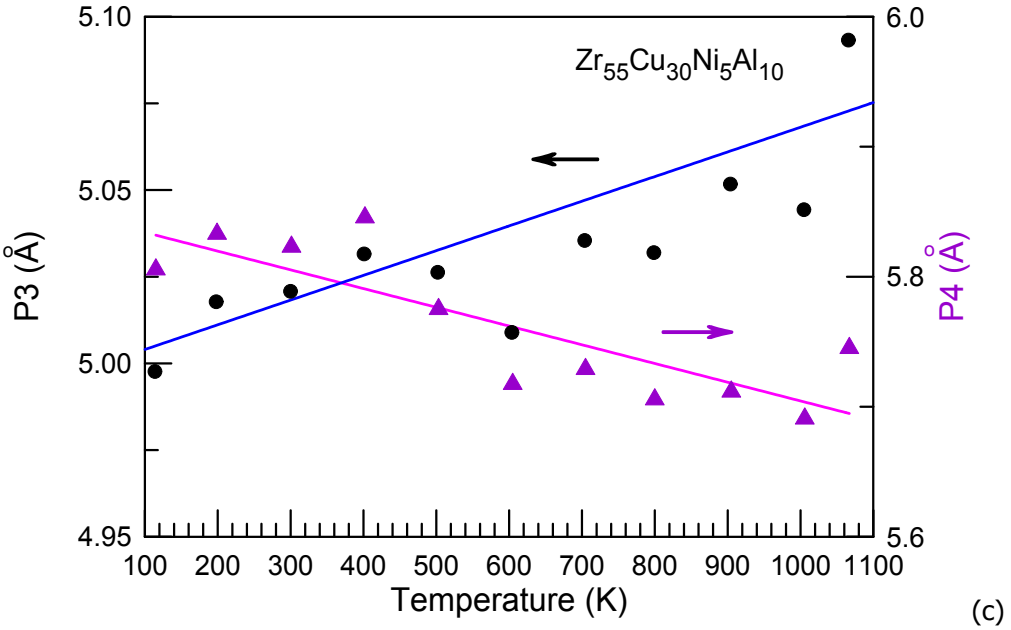

Fig. 3. Positions of P1 and P2 in the first coordination shell (a) and the ratio of the corresponding peak areas (*AP1/AP2*) (b) as a function of temperature (a,b) and inverse temperature in (b). The positions of P3 and P4 as a function of temperature (c). The arrows in (a and c) indicate Y-axes corresponding to the data while the arrows in (b) indicate the corresponding X-axes. The insert in (a) is schematic representation of atomic redistribution within and between the first and higher order coordination shells leading to continuous structure changes in metallic liquids on heating and cooling leading to redistribution of the atomic number density as indicated by the red double side arrow.

As it has been already mentioned before, seven Gaussian function peaks represent very well the entire shape of *G(R)* (Fig. 2a). However, in the earlier works it was shown that owing to a complex asymmetrical shape of the first peak the maximum of *G(R)* does not necessarily characterize all interatomic distances and the entire shape of the first peak should be taken into consideration [82,83]. As one can see in Fig. 1b in addition to intensification of 4 sub-peaks marked with arrows there is a decrease in the fraction of high *R* value atomic pairs in the first coordination shell (from 0.35 to 0.4 nm, see downward-left arrow) on cooling which is missed when the baseline is corrected. Nevertheless the Gaussian fitting peaks positions represent the most probable interatomic distances. Also, although

the positions of the maxima in the first coordination shell are strongly influenced by the asymmetry of the interatomic potentials (steeper slope at lower R) no shift is observed in the average atomic position ((P3+P4)/2) in the 2nd coordination shell which is much less affected by the potential.

Also, the area under the first maximum (see Fig. 2) after the baseline correction was integrated and the point corresponding to 50 % of the integrated area (R^i_{50}) (the areas of under the curve below (A1) and above this value (A2) are equal as shown in Fig. 2b) was found in a wide temperature range below the liquidus temperature. As a result on cooling the R^i_{50} position changes insignificantly from 0.303 to 0.304 nm. The change in R^i_{50} is smaller than those obtained by the Gaussian fitting (Fig. 3a) but the tendency is same – larger R^i_{50} values are found at lower temperatures. On the other hand integration of the total area under P1 and P2 in the first coordination shell of the radial distribution function (*RDF*) at 501 K indicates the coordination number (*CN*) of 13.3, a local *RDF* maximum (RDF_m) at 0.317 nm and R^i_{50}=0.312 nm, while at 1335 K *CN*=13.0, RDF_m at 0.313 nm and R^i_{50}=0.315 nm. Opposite variation in RDF_m and R^i_{50} also indicate structural modification in the liquid phase on cooling.

Owing to chemical and size similarity between Cu and Ni this quaternary alloy can be considered as a pseudo ternary Zr-(Cu,Ni)-Al one. Then, there are 6 atomic pairs in the studied alloy with distinct interatomic distances. The interatomic distances in the first coordination shell correspond to the sums of the Goldschmidt atomic radii of r_{Zr}=0.160 nm, r_{Cu}=0.128 nm, r_{Ni}=0.125 nm and r_{Al}=0.143 nm [84]. The first sub-peak (P1) in the first coordination shell corresponds to the nearest Zr-(Cu,Ni) distances (r_{Zr+Cu}=0.288 nm) while the second sub-peak (P2) mostly corresponds to that of Zr-Zr pair (r_{Zr+Zr}=0.320 nm) (Figs. 2a and 3a). The experimental peak position values are slightly lower than those predicted by the sum of the Goldschmidt atomic radii owing to formation of chemical bonds. Zr-Al interatomic distances are also closer to the value for the second peak and modify its position.

These findings imply the possible structural changes and atomic redistributions within and between the coordination shells as schematically shown in the inset of Fig. 3a. Several clusters are located around the central one. The atoms which are considered as the solute-centering are black

while surrounding atoms are white. Red circles schematically illustrate the first, second and third atomic coordination shells. Red arrow indicates permanent atomic number density redistribution between the corresponding shells on cooling. One should keep in mind that such a planar representation of the atomic structure is oversimplification and can be redrawn by using any other atom as the central one because any atom in the structure is a center of its own atomic cluster with a unique atomic arrangement, interatomic distances and a certain number of nearest neighbors. *G(R)* indicates statistically average atomic structure where maxima correspond to the most popular interatomic distances. Nevertheless this picture gives a visual representation of the structural processes occurring in a metallic fluid on cooling.

On subsequent heating of the glassy sample vitrified on cooling the change of slope of temperature dependence of the first and second peaks (P1 and P2) takes place at about 500 K indicating densification of the glassy phase. This temperature corresponds well to the temperature of beginning of structural relaxation of the glassy phase on heating.

As in case of the Pd-Cu-Ni-P alloy studied earlier [45] *AP1/AP2* (the area under P1 divided by the area under P2) ratio is nearly constant in the equilibrium liquid state. However, it changes on cooling in the supercooled liquid state (Fig. 3a). It indicates that the number of Zr-Cu and Zr-Ni atomic pairs increases on cooling below T_l owing to chemical ordering.

It is important to note that the changes in *AP1/AP2* ratio (*APR*) for the $Zr_{55}Cu_{30}Ni_5Al_{10}$ liquid alloy from T_l to T_g (the ratio in Fig. 3 is 0.30/0.12=2.5) are smaller in the absolute values compared to those found in the $Pd_{40}Cu_{30}Ni_{10}P_{20}$ liquid alloy (0.09/0.02=4.5) [45]. The *AP1/AP2* ratio values normalized per Kelvin (APR^n) according to the supercooled liquid region on cooling (T_l-T_g) are 0.005 (APR^n=2.5/530 K^{-1}) and 0.017 (APR^n=4.5/270 K^{-1}), respectively. This fact is in line with a lower fragility of the $Zr_{55}Cu_{30}Ni_5Al_{10}$ melt compared to that of the $Pd_{40}Cu_{30}Ni_{10}P_{20}$ one. Continuous structural changes in the supercooled liquid leading to the formation of atomic clusters likely change the activation energy for viscous flow, and thus, determine fragility of this glass-forming liquid through the equations (1 and 4).

Fragility of liquids also correlates with the difference in the specific heat capacity (C_p) at T_g between the liquid and glassy phases [85]. The $Zr_{55}Cu_{30}Ni_5Al_{10}$ has C_p values for liquid (C_p^l) and glassy (C_p^g) phases at T_g of about 38 and 28 J/mol·K, respectively, [86] while these values for the $Pd_{42.5}Cu_{30}Ni_{7.5}P_{20}$ alloy are 45 and 28 J/mol·K, respectively [87]. Thus, ΔC_p^{l-g} values of 10 and 17 J/mol·K for $Zr_{55}Cu_{30}Ni_5Al_{10}$ and $Pd_{42.5}Cu_{30}Ni_{7.5}P_{20}$ alloys, respectively, also correlate with a larger fragility of the latter alloy. As melting enthalpy of $Zr_{55}Cu_{30}Ni_5Al_{10}$ is close to 7.5 kJ/mol and the liquidus temperature is about 1150 K [72,73] its melting entropy (ΔS_m) is about 6.5 J/K·mol. The resulted thermodynamic fragility m_t parameter calculated using the formula:

$$m_t = 37.5 \cdot \Delta C_p / \Delta S_m \quad (5)$$

[85] is 58. For an alloy close in composition to the $Pd_{42.5}Cu_{30}Ni_{7.5}P_{20}$ one melting enthalpy is close to 5 kJ/mol [88] which gives ΔS_m of 6.1 J/K·mol. The resulted m parameter is 104. If one uses ΔS_m of 8.03 J/K·mol [89] then m=79 which is still higher than m=58 found for the $Zr_{55}Cu_{30}Ni_5Al_{10}$ alloy.

PDF(R) curves produced by MD simulation are shown in Fig. 4. Here the split of the peaks corresponding to first and second coordination shells is less visible owing to insufficient structure relaxation.

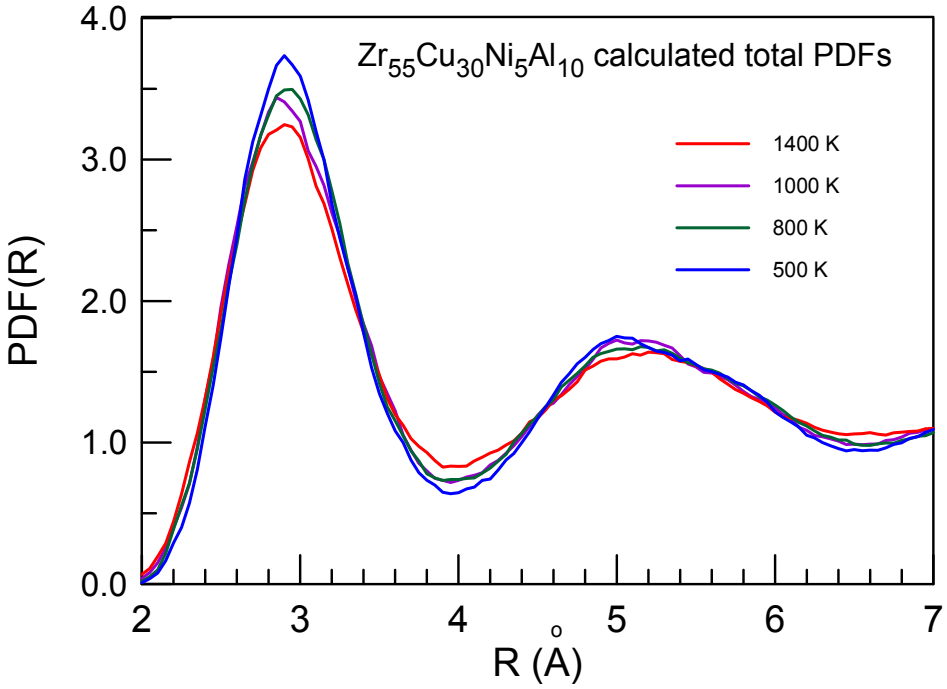

Fig. 4. *G(R)* calculated by using ab-initio MD simulation. The curves were smoothed over 10 points.

The partial *PDF(R)* functions shown in Fig. 5 indicate intensification of the Zr-Cu subpeak on cooling. The peak positions also correspond well to those obtained experimentally in Figs. 2a and 3a. On cooling there is a change in partial pair distribution functions position fitted by the Gaussian function, background subtracted. The results for two major atomic contributions are shown in Table 1. One can see the shift of Zr-Cu and Zr-Zr peaks to a higher *R* value on cooling. Intensification of both Zr-Zr and Zr-Cu peaks (area) is also observed.

Table 1. Position and area of two Zr-Zr and Zr-Cu peaks at two temperatures.

Temperature, K	Zr-Zr		Zr-Cu	
	R, nm	Area	R, nm	Area
1400 K	0.3185	0.788	0.2850	1.022
500 K	0.3225	0.850	0.2860	1.094

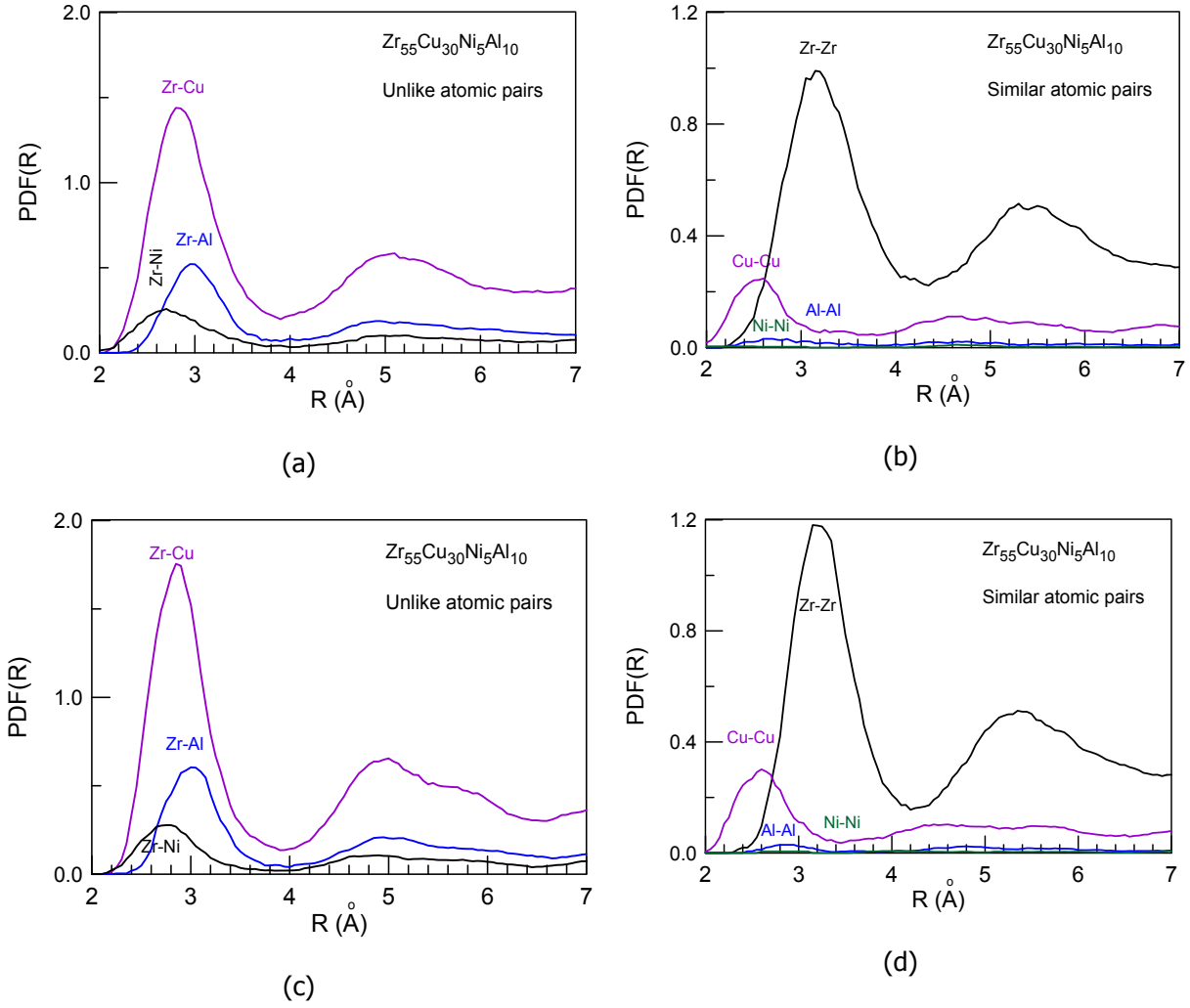

Fig. 5. Partial *PDF(R)* functions obtained by computer simulation at 1400 K (liquid state) (a,b) and 500 K (glass state) (c,d).

Moreover, as shown in Fig. 6, the calculated partial densities of states (PDOS) (corresponding to the 3s, 3p, 3d and 4d states of Al, Ni, Cu and Zr atoms), respectively, indicate some changes in the electronic structure towards a short range order formation in the glass. The redistribution of peak intensities for Ni and Cu is found on cooling. Broader peak distributions of electron density below the Fermi level corresponding to Cu and Ni atoms are observed in the liquid state. It is interesting that the most significant changes are found in the peak shape of Ni in the energy region from -3.0 to -1.0 eV. During the cooling process, the redistribution of peak intensities for Ni atoms occurred by shifting the

electron density to a narrower region between -3.0 and -2.0 eV. It indicates the formation of stronger bonds with Ni atoms.

The *s* and *p* electron orbitals of Al overlap with those of all other elements thus stabilizing the glassy structure. This fact may be related to a higher glass forming ability of ternary Zr-Cu-Al metallic alloys compared to binary Zr-Cu alloys. For example, PDOS of Zr and Cu are much less overlapped.

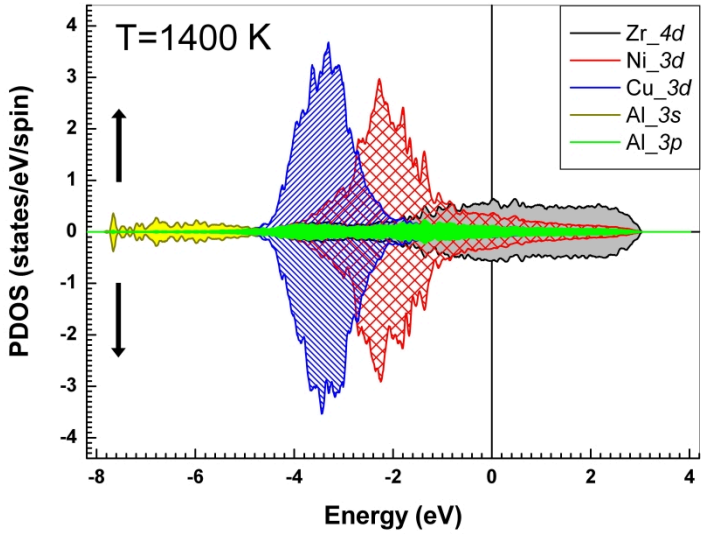

(a)

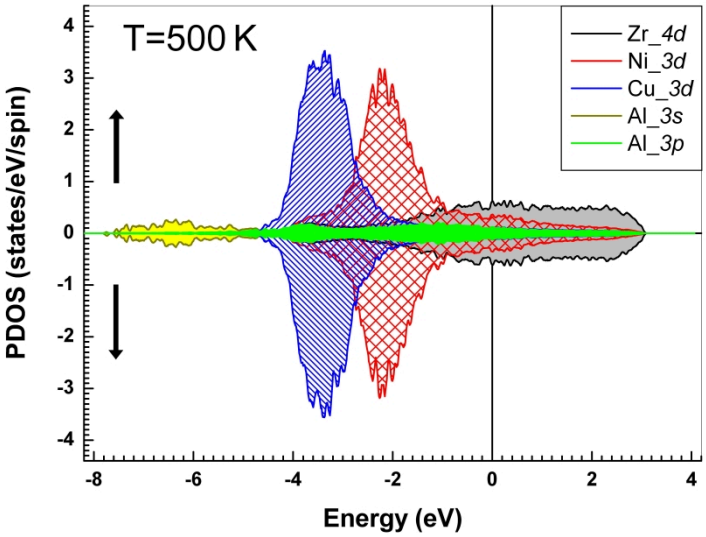

(b)

Fig. 6. PDOS for the spin-up (↑) and spin-down (↓) as shown, at T= 1400 K (a) and at T= 500 K (b) respectively. The Fermi level (vertical line) has been chosen as zero energy.

The Voronoi polyhedral analysis was also applied to the cells. However, owing to small cell sizes no systematic variation in coordination numbers of the polyhedral clusters is found with temperature except for Ni with *CN*=12. The number of Ni-centered clusters with *CN*=12 increased from 5 to 10 to 12 on cooling from 1400 to 500 K. This is in line with intensification of the Ni PDOS peak in Fig. 6 indicating formation of Ni-centered clusters.

4. Conclusion

According to the results strong chemical ordering forming Zr-Cu,Ni, Zr-Al and Zr-Zr atomic pairs takes place in the $Zr_{55}Cu_{30}Ni_5Al_{10}$ supercooled liquid alloy on cooling below the liquidus temperature. However, here the change in the Zr-Cu,Ni peak area to other peaks area ratio (APR and APR^n) is smaller than in case of the Pd-Cu-Ni-P alloy studied earlier (Cu,Ni-P to other peaks) in accordance with a lower fragility index of the $Zr_{55}Cu_{30}Ni_5Al_{10}$ melt. It is concluded that fragility is a sign of instability of short and medium range order in fragile liquids. MD simulation was found to support the observed structure variation as a function of temperature and indicated intensification of Zr-Cu, Zr-Al and Zr-Zr interactions on cooling.

Acknowledgement:

This paper is dedicated to the memory of our wonderful colleague Alain Resa Yavari who started this research but passed away before it was completed. D.L. gratefully acknowledges financial support received from the World Premier International Research Center Initiative (WPI), MEXT, Japan. R.V.B. is grateful to the crew of Center for Computational Materials Science and E-IMR center at the Institute for Materials Research, Tohoku University, for continuous support.

References

[1] C. Suryanarayana and A. Inoue, Bulk metallic glasses, Second Edition, 2017, p. 520.

[2] D. V. Louzguine-Luzgin, Metallic glasses and those composites, Materials Research Forum LLC, Millersville, PA, USA, (2018) p. 336.

[3] M. Petrzhik, V. Molokanov, E. Levashov, On conditions of bulk and surface glass formation of metallic alloys, Journal of Alloys and Compounds, 707 (2017) 68-72.

[4] D.V. Louzguine-Luzgin, J. Jiang, On long-term stability of metallic glasses, Metals, 9 (2019) 1076.

[5] V.V. Molokanov and V.N. Chebotnikov, Glass forming ability, structure and properties of Ti and Zr-intermetallic compound based alloys, Key Engineering Materials, 40-41 (1990) 319-332.

[6] S. Sato, T. Sanada, J. Saida, M. Imafuku, E. Matsubara and A. Inoue, Effect of Al on local structures of Zr–Ni and Zr–Cu metallic glasses, Materials Transactions, 46 (2005) 2893-2897.

[7] J. Antonowicz, D.V. Louzguine-Luzgin, A.R. Yavari, K. Georgarakis, M. Stoica, G. Vaughan, E. Matsubara, A. Inoue, Atomic structure of Zr-Cu-Al and Zr-Ni-Al amorphous alloys, Journal of Alloys and Compounds, 471 (2009) 70-73.

[8] N. E. Dubinin, N. A. Vatolin, and V. V. Filippov, Thermodynamic perturbation theory in studies of metal melts, Russian Chemical Reviews, 83 (2014) 987-1002.

[9] D. Bolmatov, V. V. Brazhkin and K. Trachenko, The phonon theory of liquid thermodynamics, Scientific Reports, 2 (2012) 421.

[10] C. A. Angell, Relaxation in liquids, polymers and plastic crystals—strong/fragile patterns and problems, J. Non-Cryst. Solids, 131 (1991) 13–31.

[11] T. Egami, Real-space description of dynamics of liquids, Quantum Beam Sci. 2 (2018) 22.

[12] W. F. Gale, T. C. Totemeier, Smithells Metals Reference Book 8-th ed, Elsevier Butterworth-Heinemann Ltd., Oxford UK, 2004, 14-1.

[13] M. E. Blodgett, T. Egami, Z. Nussinov and K. F. Kelton, Proposal for universality in the viscosity of metallic liquids, Sci. Rep. 5 (2015) 13837.

[14] C. A. Angell, Relaxation in liquids, polymers and plastic crystals - strong/fragile patterns and problems, *J. Non-Cryst. Solids*, 131-133 (1991) 13.

[15] L. Hu and X. F. Bian, Liquid fragility. A key to going deep into materials of glassy states, Chinese Science Bulletin, 49 (2004) 1-9.

[16] P.S. Popel and Y.E. Sidorov, Microheterogeneity of liquid metallic solutions and its influence on the structure and properties of rapidly quenched alloys, Materials Science and Engineering A, 226-228 (1997) 237-244.

[17] U. Dahlborg, M. Calvo-Dahlborg, P.S. Popel, and V.E. Sidorov, Structure and properties of some glass-forming liquid alloys, Eur. Phys. J. B, 14 (2000) 639-648.

[18] V.A. Polukhin, N.I. Sidorov, N.A. Vatolin, Presolidification changes in the structural–dynamic characteristics of glass-forming metallic melts during deep cooling, vitrification, and hydrogenation, Russian Metallurgy (Metally), 8 (2019) 758-780.

[19] P.S. Popel, LG. Brodova, V.M. Zamjatin, I.V. Polentz, V.O. Esin and A.I. Moisejev, Conditions for the formation of metastable phases during crystallization of Al-Zr alloys, Rasplavy, 2 (1988) 23 (in Russian).

[20] O. Mishima, & H. E. Stanley, The relationship between liquid, supercooled and glassy water, Nature, 396 (1998) 329–335.

[21] Y. Katayama, T. Mizutani, W. Utsumi, O. Shimomura, M. Yamakata and K.I. Funakoshi, A first-order liquid–liquid phase transition in phosphorus, Nature, 403 (2000) 170.

[22] M. Kobayashi and H. Tanaka, The reversibility and first-order nature of liquid–liquid transition in a molecular liquid, Nature Communications, 7 (2016) 13438.

[23] T. Morishita, Liquid-liquid phase transitions of phosphorus via constant-pressure first-principles molecular dynamics simulations, Phys. Rev. Lett., 87 (2001) 105701.

[24] M. Stolpe, I. Jonas, S. Wei, Z. Evenson, W. Hembree, F. Yang, A. Meyer, and R. Busch, Structural changes during a liquid-liquid transition in the deeply undercooled $Zr_{58.5}Cu_{15.6}Ni_{12.8}Al_{10.3}Nb_{2.8}$ bulk metallic glass forming melt, Phys. Rev. B, 93 (2016) 014201.

[25] W.T. Laughlin and D.R. Uhlmann, Viscous flow in simple organic liquids, J. Phys. Chem., 76 (1972) 2317-2325.

[26] C. A. Angell, Formation of glasses from liquids and biopolymers, Science, 267 (1995) 1924.

[27] D. V. Louzguine-Luzgin, L. V. Louzguina-Luzgina, H.J. Fecht, On limitations of the viscosity versus temperature plot for glass-forming substances, Materials Letters, 182 (2016) 355–358.

[28] M. Ikeda and M. Aniya, Analysis and characterization of the transition from the Arrhenius to non-Arrhenius structural relaxation in fragile glass-forming liquids, Journal of Thermal Analysis and Calorimetry, 132 (2018) 835–842.

[29] L. M. Martinez and C. A. Angell, A thermodynamic connection to the fragility of glass-forming liquids, Nature, 410 (2001) 663-667.

[30] L. M. C. Janssen, P. Mayer, and D. R. Reichman, Relaxation patterns in supercooled liquids from generalized mode-coupling theory, Phys. Rev. E 90, (2014) 052306.

[31] O. N. Senkov, Correlation between fragility and glass-forming ability of metallic alloys, Phys. Rev. B, 76 (2007) 104202.

[32] D. V. Louzguine-Luzgin, N. Chen, A. Yu. Churymov, L. V. Louzguina-Luzgina, V. I. Polkin, L. Battezzati and A. R. Yavari, Role of different factors in the glass-forming ability of binary alloys, Journal of Materials Science, 50 (2015) 1783-1793.

[33] W. L. Johnson, J. H. Na and M. D. Demetriou, Quantifying the origin of metallic glass formation, Nat. Commun. 7 (2016) 10313.

[34] T. Scopigno, G. Ruocco, F. Sette, G. Monaco, Is the fragility of a liquid embedded in the properties of its glass? Science, 302 (2003) 849-852.

[35] W. L. Johnson, J. H. Na and M. D. Demetriou, Quantifying the origin of metallic glass formation, Nat. Commun., 7 (2016) 10313.

[36] W. Kim, H.S. Oh and E.S. Park, Manipulation of thermal and mechanical stability by addition of multiple equiatomic rare-earth elements in Al-TM-RE metallic glasses, Intermetallics 91 (2017) 8–15.

[37] Y. Kawamura and A. Inoue, Newtonian viscosity of supercooled liquid in a $Pd_{40}Ni_{40}P_{20}$ metallic glass, Appl. Phys. Lett., 77 (2000) 1114.

[38] M. H. Cohen and G. S. Grest, Liquid-glass transition, a free-volume approach, Phys. Rev. 20, (1979) 1077.

[39] M.I. Ojovan, Ordering and structural changes at the glass–liquid transition, Journal of Non-Crystalline Solids, 382 (2013) 79–86.

[40] M. I. Ojovan, Viscous flow and the viscosity of melts and glasses, Phys. Chem. Glasses: Eur. J. Glass Sci. Technol. B, 53 (2012) 143–150.

[41] D.S. Sanditov and M.I. Ojovan, Relaxation aspects of the liquid-glass transition, Physics-Uspekhi, 62 (2019) 111-130.

[42] K. F. Kelton, Kinetic and structural fragility - A correlation between structures and dynamics in metallic liquids and glasses, Journal of Physics Condensed Matter, 29 (2017) 023002.

[43] G. J. Fan, J. F. Löffler, R. K. Wunderlich, H. J. Fecht, Thermodynamics, enthalpy relaxation and fragility of the bulk metallic glass-forming liquid $Pd_{43}Ni_{10}Cu_{27}P_{20}$, Acta Materialia, 52 (2004) 667.

[44] D. V. Louzguine-Luzgin, A. I. Bazlov, A. Yu. Churyumov, K. Georgarakis, and A. R. Yavari, Comparative analysis of the structure of palladium-based bulk metallic glasses prepared by treatment of melts with flux, Physics of the Solid State, 55 (2013) 1985–1990.

[45] D. V. Louzguine-Luzgin, R. Belosludov, A. R. Yavari, K. Georgarakis, G. Vaughan, Y. Kawazoe, T. Egami and A. Inoue, Structural basis for supercooled liquid fragility established by synchrotron-radiation method and computer simulation, Journal of Applied Physics, 110 (2011) 043519.

[46] N.A. Mauro, M.L. Johnson, J.C. Bendert, K.F. Kelton, Structural evolution in Ni–Nb and Ni–Nb–Ta liquids and glasses — A measure of liquid fragility? Journal of Non-Crystalline Solids, 362 (2013) 237.

[47] N. A. Mauro, M. Blodgett, M. L. Johnson, A. J. Vogt and K. F. Kelton, A structural signature of liquid fragility, Nature Communications, 5 (2014) 4616.

[48] A.K. Gangopadhyay and K.F. Kelton, Recent progress in understanding high temperature dynamical properties and fragility in metallic liquids, and their connection with atomic structure, Journal of Materials Research, 32 (2017) 2638-2657.

[49] A. R. Yavari, A. Le Moulec, A. Inoue, N. Nishiyama, N. Lupu, E. Matsubara, W. J. Botta, G. Vaughan, M. Di Michiel, A. Kvick, Excess free volume in metallic glasses measured by X-ray diffraction, *Acta Materialia*, 53 (2005) 1611.

[50] A. Mizuno, S. Matsumura, M. Watanabe, S. Kohara, M. Takata, High-energy x-ray diffraction study of liquid structure of metallic glass-forming $Zr_{70}Cu_{30}$ alloy, Materials Transactions, 46 (2005) 2799-2802.

[51] D.D. Qu, A. Mizuno, M. Watanabe, J. Bednarcik, J. Shen, Undercooling behavior of Zr–Cu–Ni–Al bulk metallic glasses investigated by in situ synchrotron high energy X-ray diffraction, Mater. Sci. Eng. A, 555 (2012) 36-43.

[52] D. V. Louzguine and A. Inoue, Formation of a nanoquasicrystalline phase in Zr-Cu-Ti-Ni metallic glass, Applied Physics Letters, 78 (2001) 1841-1843.

[53] A.S. Aronin, G.E. Abrosimova, A.F. Gurov, Yu.V. Kir'yanov, V.V. Molokanov, Nanocrystallization of bulk Zr-Cu-Ti metallic glass, Materials Science and Engineering A, 304-306 (2001) 375-379.

[54] R.V. Belosludov, A.I. Oreshkin, S.I. Oreshkin, D.A. Muzychenko, H. Kato, D.V. Louzguine-Luzgin, The atomic structure of a bulk metallic glass resolved by scanning tunneling microscopy and ab-initio molecular dynamics simulation, Journal of Alloys and Compounds, 816 (2020) 152680.

[55] D.V. Louzguine-Luzgin, M. Ito, S.V. Ketov, A.S. Trifonov, J. Jiang, C.L. Chen, K. Nakajima, Exceptionally high nanoscale wear resistance of a $Cu_{47}Zr_{45}Al_8$ metallic glass with native and artificially grown oxide, Intermetallics, 93 (2018) 312-317.

[56] K. Georgarakis, L. Hennet, G.A. Evangelakis, J. Antonowicz, G.B. Bokas, V. Honkimaki, A. Bytchkov, M.W. Chen and A.R. Yavari, Probing the structure of a liquid metal during vitrification, Acta Materialia, 87 (2015) 174-186.

[57] D. V. Gunderov, E. V. Boltynjuk, E. V. Ubyivovk, A. A. Churakova, G. E. Abrosimova, V. D. Sitdikov, A. R. Kilmametov and R. Z. Valiev, High pressure torsion induced structural transformations in Ti- and Zr-based amorphous alloys, IOP Conference Series Materials Science and Engineering, 447 (2018) 012052.

[58] G. E. Abrosimova, A. S. Aronin, N. S. Afonikova, and N. P. Kobelev, Influence of deformation on the structural transformation of the $Pd_{40}Ni_{40}P_{20}$ amorphous phase, Physics of the Solid State, 52 (2010) 1892–1898.

[59] M.I. Mendelev, M.J. Kramer, R.T. Ott, D.J. Sordelet, M.F. Besser, A. Kreyssig, Experimental and computer simulation determination of the structural changes occurring through the liquid–glass transition in Cu–Zr alloys, Philosophical Magazine, 90 (2010) 3795-3815.

[60] C.E. Lekka, G.B. Bokas, G.A. Almyras, D.G. Papageorgiou, G.A. Evangelakis, Clustering, microalloying and mechanical properties in Cu/Zr-based glassy models by molecular dynamics simulations and ab-initio computations, Journal of Alloys and Compounds, 536 (2012) S65-S69.

[61] Y. Q. Cheng, E. Ma, and H. W. Sheng, Alloying strongly influences the structure, dynamics, and glass forming ability of metallic supercooled liquids, Appl. Phys. Lett., 93 (2008) 111913.

[62] Y. Yokoyama, E. Mund, A. Inoue and L. Schultz, Production of $Zr_{55}Cu_{30}Ni_5Al_{10}$ glassy alloy rod of 30mm in diameter by a cap-cast technique, Materials Transactions, 48 (2007) 3190-3192.

[63] T. Yamasaki, S. Maeda, Y. Yokoyama, D. Okai, T. Fukami, H. M. Kimura and A. Inoue, Viscosity measurements of $Zr_{55}Cu_{30}Al_{10}Ni_5$ and $Pd_{40}Cu_{30}Ni_{10}P_{20}$ supercooled liquid alloys by using a penetration viscometer, Materials Transactions, 46 (2005) 2746-2750.

[64] J. C. Qiao and J. M. Pelletier, Mechanical relaxation in a Zr-based bulk metallic glass: Analysis based on physical models, J. Appl. Phys., 112 (2012) 033518.

[65] O. Haruyama, K. Yoshikawa, Y. Yamazaki, Y. Yokoyama and T. Egami, Comparison of structural relaxation behavior in as-cast and pre-annealed Zr-based bulk metallic glasses just below glass transition, Materials Transactions, 56 (2015) 648-654.

[66] L. Hennet, V. Cristiglio, J. Kozaily, I. Pozdnyakova, H.E. Fischer, A. Bytchkov, J.W.E. Drewitt, M. Leydier, D. Thiaudiere, S. Gruner, S. Brassamin, D. Zanghi, G.J. Cuello, M. Koza, S. Magazu, G.N. Greaves, D.L. Price, Aerodynamic levitation and laser heating: applications at synchrotron and neutron sources, Eur. Phys. J. Spec. Top., 196 (2011) 151-165.

[67] Y. Waseda, The structure of non-crystalline materials, McGraw-Hill, New York, (1980) p. 670.

[68] O. Haruyama, Y. Nakayama, R. Wada, H. Tokunaga, J. Okada, T. Ishikawa, Y. Yokoyama, Volume and enthalpy relaxation in $Zr_{55}Cu_{30}Ni_5Al_{10}$ bulk metallic glass, Acta Materialia, 58 (2010) 1829–1836.

[69] G. Kresse, J. Furthmuller, Efficient iterative schemes for ab initio total-energy calculations using a plane-wave basis set, Phys. Rev. B, 54 (1996) 11169.

[70] J. P. Perdew, K. Burke, M. Ernzerhof, Generalized gradient approximation made simple, *Phys. Rev. Lett.,* 77 (1996) 3865.

[71] P. E. Blöchl, Projector augmented-wave method, *Phys. Rev. B,* 50 (1994) 17953.

[72] O. Haruyama, Y. Nakayama, R. Wada, H. Tokunaga, J. Okada, T. Ishikawa, Y. Yokoyama, Volume and enthalpy relaxation in $Zr_{55}Cu_{30}Ni_5Al_{10}$ bulk metallic glass, Acta Materialia 58 (2010) 1829–1836.

[73] R. A. Sergiienko, O. A. Shcheretskyi, V. Yu. Zadorozhnyy, A. M. Verkhovliuk, D. V. Louzguine-Luzgin, Investigation of $Zr_{55}Cu_{30}Al_{10}Ni_5$ bulk amorphous alloy crystallization, Journal of Alloys and Compounds, 791 (2019) 477-482.

[74] N. Mattern, H. Hermann, S. Roth, J. Sakowski, M. P. Macht, P. Jovari, J. Jiang, Structural behavior of $Pd_{40}Cu_{30}Ni_{10}P_{20}$ bulk metallic glass below and above the glass transition, *Appl. Phys. Lett.,* 82 (2003) 2589.

[75] K. Georgarakis, D. V. Louzguine-Luzgin, J. Antonowicz, G. Vaughan, A. R. Yavari, T. Egami, A. Inoue, Variations in atomic structural features of a supercooled Pd–Ni–Cu–P glass forming liquid during in situ vitrification, Acta Materialia*,* 59 (2011) 708.

[76] D. V. Louzguine-Luzgin, K. Georgarakis, V. Zadorozhnyy, N. Chen, K. Nakayama, G. Vaughan, A. R. Yavari and A. Inoue, Atomic structure changes and phase transformation behavior in Pd-Si bulk glass-forming alloy, Intermetallics, 20 (2012) 135-140.

[77] N. Mattern, J. Bednarcik, M. Stoica, J. Eckert, Temperature dependence of the short-range order of $Cu_{65}Zr_{35}$ metallic glass, Intermetallics, 32 (2013) 51-56.

[78] X. Tong, G. Wang, Z. H. Stachurski, J. Bednarčík, N. Mattern, Q. J. Zhai & J. Eckert, Structural evolution and strength change of a metallic glass at different temperatures, Scientific Reports 6, (2016) 30876.

[79] D. V. Louzguine-Luzgin, K. Georgarakis, A. Tsarkov, A. Solonin, V. Honkimaki, L. Hennet and A. R. Yavari, Structural changes in liquid Fe and Fe–B alloy on cooling, Journal of Molecular Liquids, 209 (2015) 233–238.

[80] A. K. Gangopadhyay, M. E. Blodgett, M. L. Johnson, J. McKnight, V. Wessels, A. J. Vogt, N. A. Mauro, J. C. Bendert, R. Soklaski, L. Yang, and K. F. Kelton, Anomalous thermal contraction of the first coordination shell in metallic alloy liquids, The Journal of Chemical Physics, 140 (2014) 044505.

[81] H. Lou, X. D. Wang, Q.P. Cao, D.X. Zhang, J. Zhang, T.D. Hu, H.K. Mao, and J.Z. Jiang, Negative expansions of interatomic distances in metallic melts, PNAS, 110 (2013) 10068-10072.

[82] J. Ding, M. Xu, P. F. Guan, S. W. Deng, Y. Q. Cheng, and E. Ma, Temperature effects on atomic pair distribution functions of melts, J. Chem. Phys. 140, (2014) 064501.

[83] S. V. Sukhomlinov, and M. H. Müser, Determination of accurate mean bond lengths from radial distribution functions, J. Chem. Phys. 146, (2017) 024506.

[84] W. F. Gale, T. C. Totemeier, Smithells Metals Reference Book 8-th ed, Elsevier Butterworth-Heinemann Ltd., Oxford UK, 2004, p. 4-44.

[85] I.S. Klein and C.A. Angell, Excess thermodynamic properties of glassforming liquids: The rational scaling of heat capacities, and the thermodynamic fragility dilemma resolved, Journal of Non-Crystalline Solids, 451 (2016) 116–123.

[86] D. V. Louzguine-Luzgin, I. Seki, T. Yamamoto, H. Kawaji, C. Suryanarayana, and A. Inoue, Double-stage glass transition in a metallic glass, Physical Review B, 81 (2010) 144202.

[87] O. Haruyama, T. Watanabe, K. Yuki, M. Horiuchi, H. Kato, and N. Nishiyama, Thermodynamic approach to glass-forming ability of water-quenched Pd-P-based and $Pt_{60}Ni_{15}P_{25}$ bulk metallic glasses, Physical Review B, 83 (2011) 064201.

[88] N. Nishiyama and A. Inoue, Supercooling investigation and critical cooling rate for glass formation in Pd-Cu-Ni-P alloy, Acta Materialia, 47 (1999) 1487-1495.

[89] J. Schroers, Y. Wu, R. Busch, W.L. Johnson, Transition from nucleation controlled to growth controlled crystallization in $Pd_{43}Ni_{10}Cu_{27}P_{20}$ melts, Acta Materialia, 49 (2001) 2773-2781.

2020-04-29

An atomistic study of the structural þÿchanges in a Zr Cu Ni Al glass liquid on vitrification monitored in-situ by X-ray diffraction and molecular dynamics simulation

Louzguine-Luzgin, D. V.

Elsevier

Louzguine DV, Georgarakis K, Andrieux J, et al., (2020) An atomistic study of the structural þÿchanges in a Zr Cu Ni Al glass-forming liquid on vitrification monitored i diffraction and molecular dynamics simulation. Intermetallics, Volume 122, July 2020, Article number 106795

https://doi.org/10.1016/j.intermet.2020.106795